(Received 27 September 2023, Accepted November 4 2023, Scheduled 24 November 2023)

The Direct Torque Control of Brushless DC Motor Based on Sliding Mode Change Structure

Gai Liu[1,*], Yiran Wu[2], and Qingbo Shao[1]

[1] Xuzhou University of Technology, Xuzhou 221018, China
[2] Southeast University Chengxian College, Nanjing 210088, China

ABSTRACT: Aiming at the problem of slow response speed and poor anti-interference ability using the traditional PI control in the direct torque control strategy of brushless DC motor (BLDCM), the direct torque control (DTC) of the BLDCM based on the sliding mode change (SMC) structure is proposed. In the BLDCM DTC system under the new flux linkage set mode, the traditional PI control is replaced by the improved SMC control to realize the new torque set mode and realize the DTC of the BLDCM. Firstly, the integral sliding mode surface is used instead of the traditional linear sliding mode surface to optimize the continuity of the SMC structure and reduce the high-frequency perturbation caused by the differential phase, thus reducing the smooth torque and system steady-state error. Secondly, the system is simulated by MATLAB/SIMULINK; the set torque of the improved SMC is the most stable; and the speed response curve is smoother. Finally, the construction of the BLDCM test platform is completed. The experimental results show that in the BLDCM DTC control system of the new flux linkage set mode, based on the improved SMC, the system has faster response speed and stronger anti-interference, and shows stronger dynamic and static performance.

1. INTRODUCTION

In general, when analyzing the permanent magnet brushless DC motor, the counter electromotive forcewaveform is trapezoidal wave, and the flat top width is 120°. Due to the process problems such as insufficient rotor magnetic charging and winding asymmetry in the manufacturing process, it is difficult to realize the ideal trapezoidal wave of the counter electromotive force waveform of the actual permanent magnet brushless DC motor. Therefore, if the current and rotational speed double closed-loop control is adopted, a large low-frequency torque pulsation and a poor dynamic performance are produced [1–3]. The direct torque control, as a high-performance brushless DC motor control strategy, can effectively suppress the low-frequency torque pulsation. Meanwhile, because the direct torque is a direct torque control, it can obtain faster torque response speed than the double closed-loop control composed of current and rotation speed.

The key technology of the direct torque control strategy is how to obtain the stator flux linkage and motor torque accurately and in real time. According to the motor theory, the electromagnetic torque of the brushless DC motor can be obtained by the calculation of the counter electromotive force, phase current, and angular velocity. The phase current and angular velocity can be measured by the corresponding sensor, but it is difficult to obtain the counter electromotive force. The direct torque control scheme for a brushless DC motor is proposed in [4], and the low-frequency torque pulse and torque dynamics are improved. Refs. [5–7] introduce the voltage space vector into the direct torque control of the brushless DC motor, the combination of flux linkage control and torque control of brushless DC motor is realized, and Refs. [8, 9] analyze the influence of the conventional reverse potential sliding mode observer and the stator inductor/resistance parameters. An adaptive sliding-mode state observer is proposed, which further improves the robustness of the system. Ref. [10] uses a sliding mode change structure state observer to estimate the inversion momentum waveform and uses an extended Kalman filter to estimate the rotational speed, which realize the direct torque control of the brushless DC motor, and the stability and robustness of the direct torque control of the brushless DC motor are improved. Refs. [11–14] propose good control methods for direct torque control, but there are problems such as complicated control methods.

The above studies have difficulties in the counter electromotive force extraction or do not consider the adverse effects of the sliding mode input error in a small range. Because the SMC structure has a flexibly designed sliding mode, and more importantly, it has nothing to do with complex parameters and external perturbations, the control idea has many advantages [15], such as fast response speed, strong robustness, and relatively simple physical realization mode.

According to the theory of state observer and change structure control theory, the DTC method of BLDCM based on SMC structure is proposed. In the BLDCM DTC system of new flux linkage, the improved SMC structure control is used instead of the traditional proportional integral (PI) control. MATLAB/SIMULINK simulate the system, and the construction of the BLDCM test platform is completed. The experimental results show that under the set torque mode based on the improved SMC, the system has not only faster response speed

* Corresponding authors: Gai Liu (lg_just@163.com).

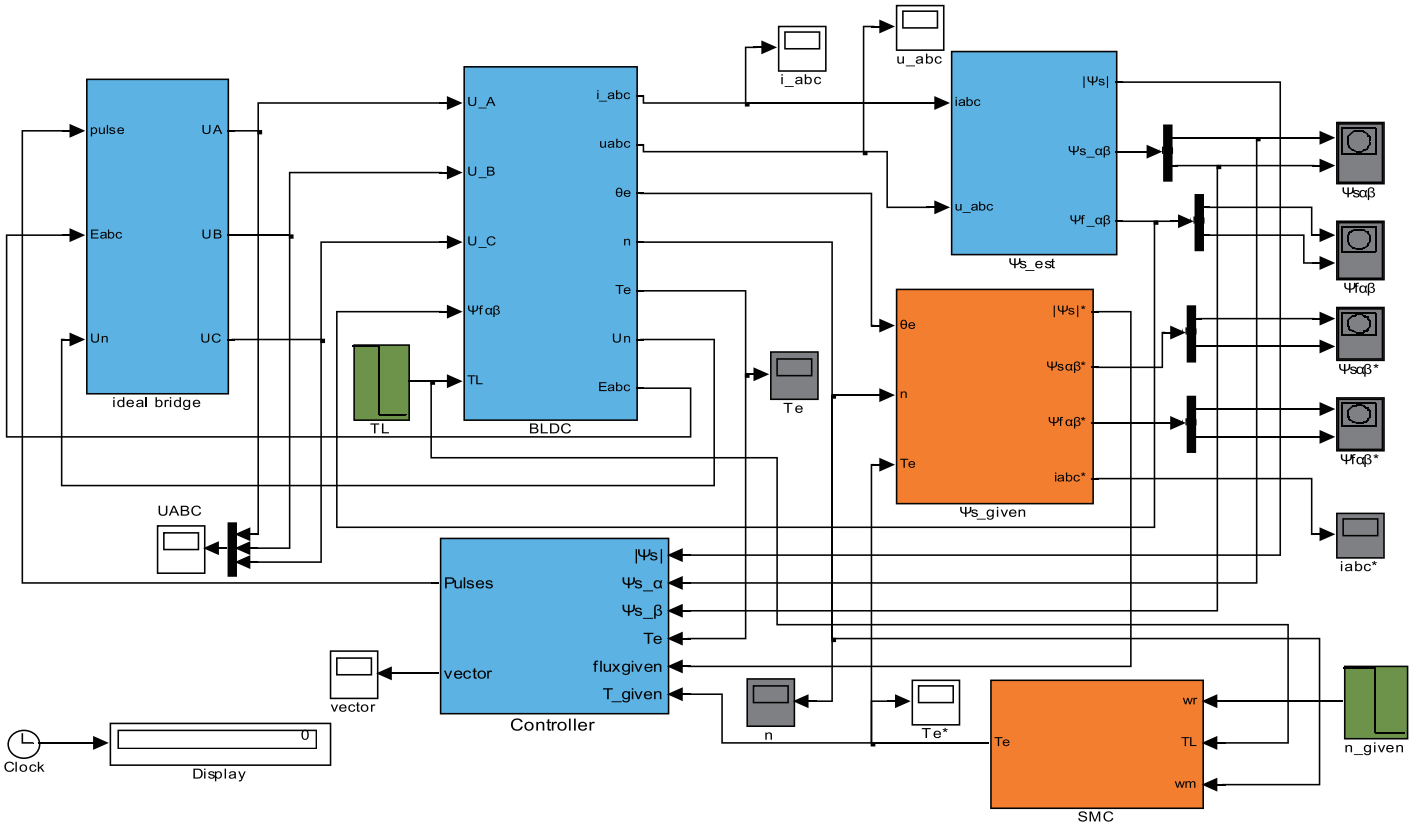

FIGURE 1. The new type of BLDCM DTC system based on sliding mode change structure.

but also stronger anti-interference, and shows stronger dynamic and static performance.

2. BRUSHLESS DC MOTOR DIRECTX TORQUE CONTROL

2.1. Brushless DC Motor Torque Calculation

The electromagnetic torque of BLDCM in the stationary coordinate system of α and β is:

$$T_e = \frac{3}{2}\frac{p}{2}\left(\frac{e_\alpha}{\omega}i_\alpha + \frac{e_\beta}{\omega}i_\beta\right) \tag{1}$$

where T_e is the electromagnetic torque of motor; p is the rotor pole number, ω is the mechanical angular velocity of the rotor; i_α, i_β, e_α, e_β are the stator current and the winding counter electromotive force in the stationary coordinates of α and β, respectively. As can be seen from the BLDCM electromagnetic torque expression, the torque calculation is related to the number of rotor poles, stator current, rotor angular velocity, and counter electromotive force, where the rotor pole number is constant, and the stator current and rotor angular velocity can be measured directly by the corresponding sensor.

2.2. Improved Design of Sliding Mode Change Structure

The design body of sliding mode controller can be summarized as two basic links: the selection of switching surface and the design of control rate. The switching function has an important impact on the dynamic quality and stability of the whole system movement. For a one-input sliding mode control system, the switching function can be expressed as follows:

$$\begin{aligned} s &= c^T x = [c_1, c_2 \cdots c_n]\begin{bmatrix} x_1 \\ x_2 \\ \vdots \\ x_n \end{bmatrix} \\ &= c_1x_1 + c_2x_2 + \cdots c_nx_n \end{aligned} \tag{2}$$

where $x_i = x^{(i-1)}$ $(i = 0, 1, 2 \ldots n)$ represent the system state and its various derivatives, respectively. When $s = 0$, the corresponding sliding mode surface can be expressed as:

$$c_1x_1 + c_2x_2 + \cdots c_nx_n = 0 \tag{3}$$

In the above equation, if the coefficient c_1c_n is a linear correlation, the order c_n value is taken as 1, then the corresponding switching function can be expressed as:

$$s = c_1x_1 + c_2x_2 + \cdots c_{n-1}x_{n-1} + x_n \tag{4}$$

The selected sliding mode switching function of the BLDCM sliding mode control adopted in this design is $s(x) = cx$, and the control system will be stable as soon as it enters the synovial area. e is defined as the difference between the set speed ω^* and the actual speed ω, namely:

$$e = \omega^* - \omega \tag{5}$$

When $c = 1$, the existing sliding mode surface function is:

$$s = \omega^* - \omega \tag{6}$$

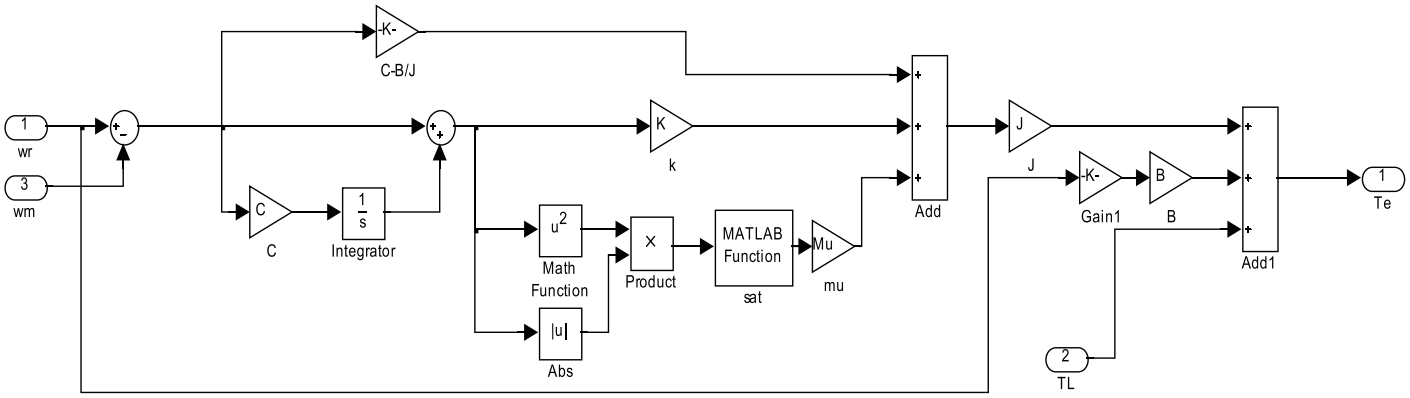

FIGURE 2. Torque set module based on improved sliding mode change structure.

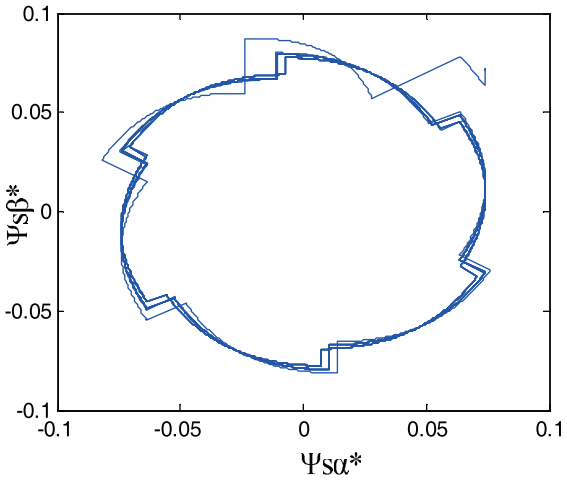

FIGURE 3. The vector locus of the set stator flux.

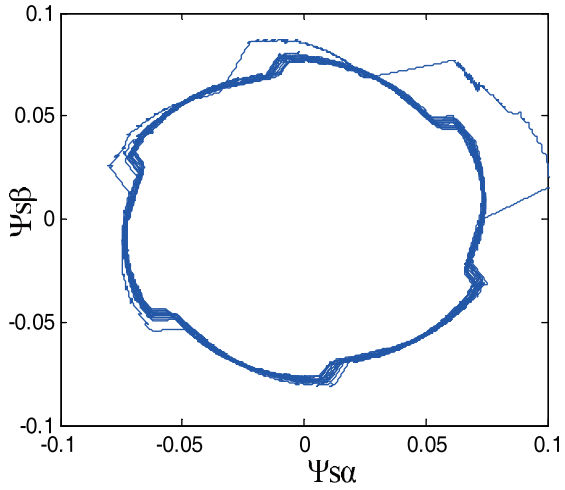

FIGURE 4. The vector locus of the actual stator flux.

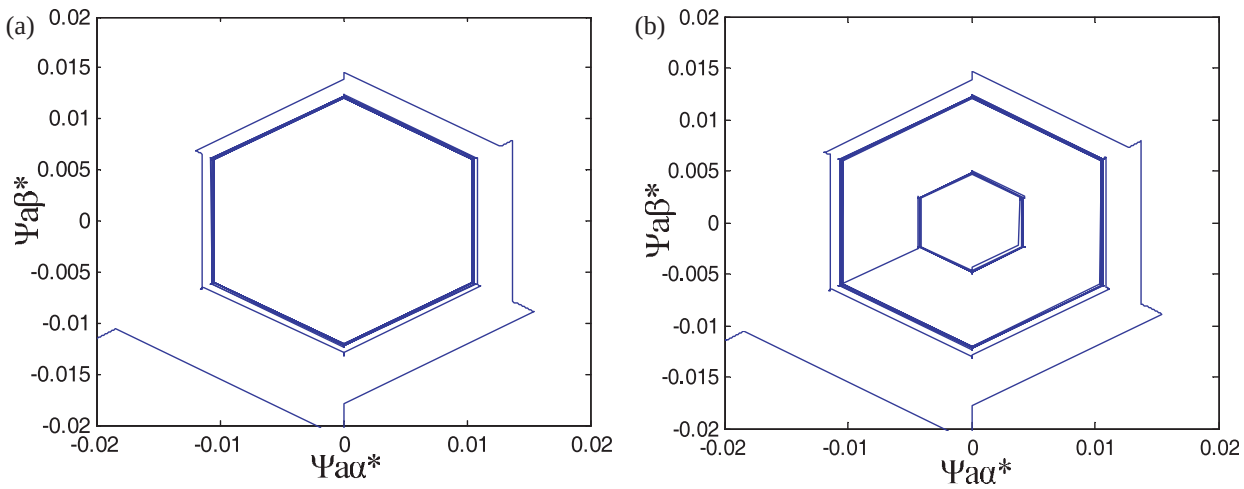

FIGURE 5. Flux linkage vector trajectory based on improved SMC. (a) Stable runtime vector trajectory. (b) Vector trajectories at load mutation.

On the sliding mode surface $s = 0$, when the time t continuously increases to infinity, ω tends to ω^*, namely, the system speed can reach the desired value and run stably. The motion equation of the motor is:

$$Te - TL = J\frac{d\omega}{dt} + Bw \tag{7}$$

Combining Equations (6) and (7), the expression is

$$\dot{s} = -\dot{\omega} = \frac{B}{J}w - \frac{1}{J}Te + \frac{1}{J}TL = ax + bu + c \tag{8}$$

where x and u are the inputs and outputs of the slide-mode controller, respectively. The functional control form adopted

TABLE 1. Main motor parameters of BLDCM.

Parameters	Values	Parameters	Values
Rated voltage U	36 V	Rotor flux linkage Ψ_f	0.0765 Wb
Rated speed n	400 rpm	Motor pole number N p	5
Rotary inertia J	0.002 N $*$ m/s^2	Stator resistance R	0.35 Ω
Counter electromotive force coefficient k_e	0.09528	Equivalent inductance L	4.64 mH

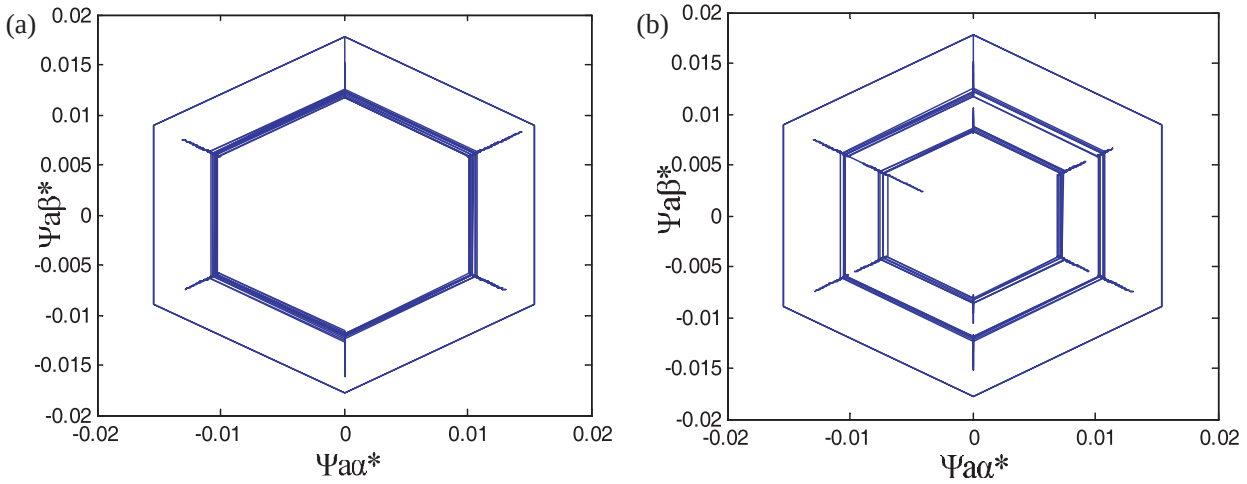

FIGURE 6. Flux linkage vector trajectory based on traditional SMC. (a) Stable runtime vector trajectory. (b) Vector trajectories at load mutation.

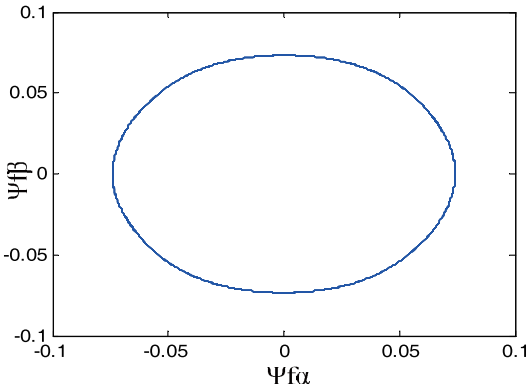

FIGURE 7. Vector track of the rotor flux.

in this design can be briefly expressed as the synthesis of the equivalent control u_{eq} and the switching control u_{sw}:

$$u = u_{eq} + u_{sw} \tag{9}$$

where the main role of the u_{eq} is to ensure the realization of the sliding-mode motion, and the main role of u_{sw} is to keep the controlled system moving closer to the sliding mode surface and reduce the impact of external uncertainty interference. Combining with formula (8) and making $\dot{s} = 0$, the equivalent control partial control rate can be obtained:

$$u_{eq} = -\frac{a}{b}x - \frac{c}{b} \tag{10}$$

In order to solve the contradiction between constant approach speed and shaking vibration, the exponential approach rate is selected:

$$\dot{s} = -\varepsilon_1 \text{sgns} - \varepsilon_2 s \quad (\varepsilon_1 > 0, \varepsilon_2 > 0) \tag{11}$$

where $\dot{s}_1 = -\varepsilon_1 \text{sgn}(s)$ is the constant approach part, and $\dot{s}_2 = -\varepsilon_2 s$ is the index part. In order to reduce the constant velocity approach rate, when approaching the sliding mode surface, the system reduces the approach speed and increases the exponential approach term. From the part of $\dot{s}_2 = -\varepsilon_2 s$, as the system approaches the sliding mode surface, its approach speed gradually decreases. When s is approximately zero, its approach velocity is also approximately zero, so it is difficult to reach the sliding mode surface in a finite time, so that the equivalent approach term is added to ensure the basic requirement of accessibility.

When $s > 0$,

$$\dot{s} = -\dot{\omega} = -\varepsilon_1 - \varepsilon_2 s \tag{12}$$

It can be drawn from the above formula:

$$s(t) = -\frac{\varepsilon_1}{\varepsilon_2} + \left(s_0 + \frac{\varepsilon_1}{\varepsilon_2}\right) e^{-\varepsilon_2 t} \tag{13}$$

In order to reduce the jitter, it is necessary to reduce the velocity value of ε_1 reaching $s = 0$ in the isovelocity approach term and improve the value of the exponential approach term ε_2 to ensure the approach speed, thus realizing the effective control of the shaking and approach speed in the traditional isovelocity rate.

Combining formula (8) and formula (11), the expression is:

$$\dot{s} = ax + bu + c = -\varepsilon_1 \text{sgns} - \varepsilon_2 s \quad (\varepsilon_1 > 0, \varepsilon_2 > 0) \tag{14}$$

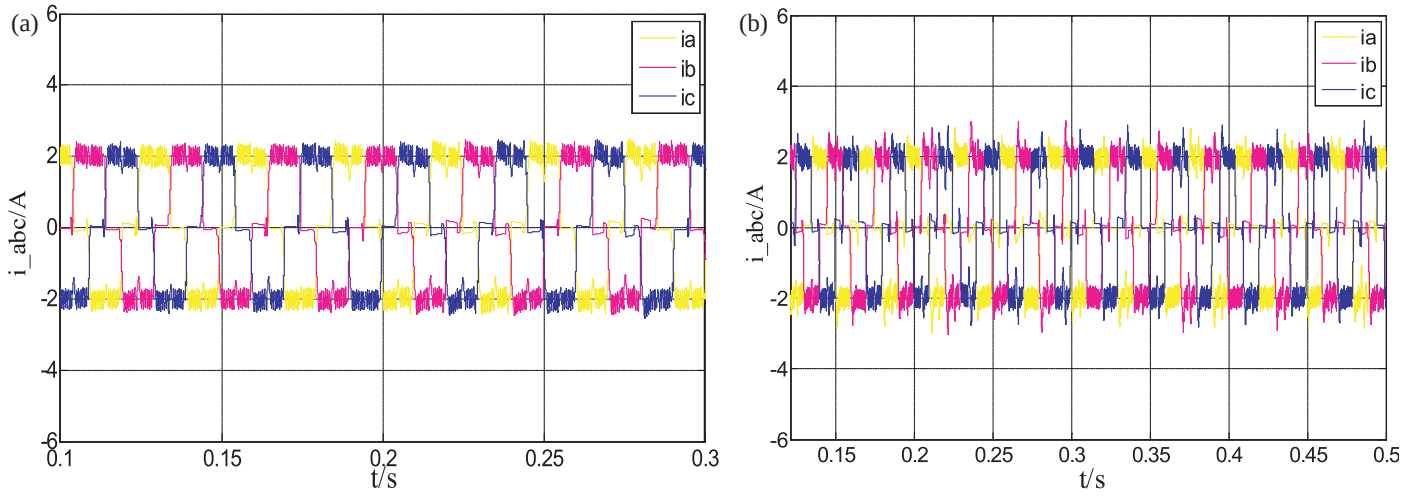

FIGURE 8. Waveform of three-phase current. (a) Based on the improved SMC. (b) Based on the PI.

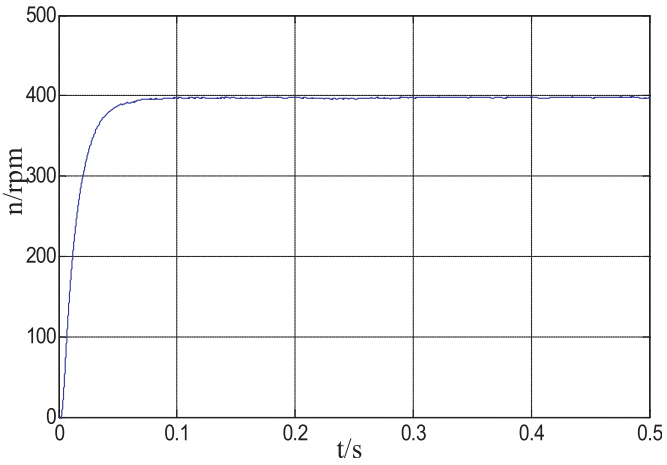

FIGURE 9. Waveform of speedbased on improved SMC.

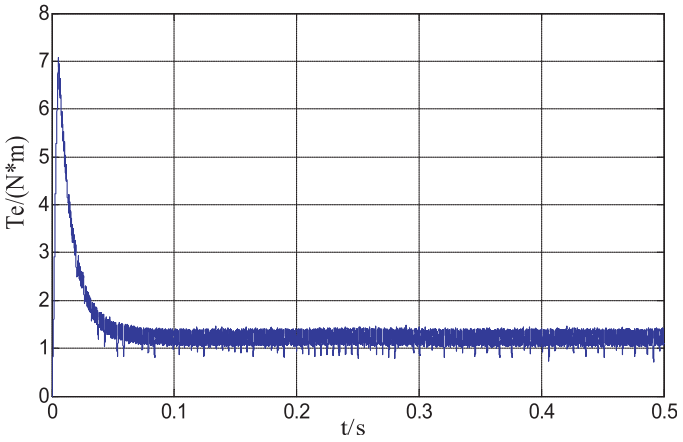

FIGURE 10. Waveform of torquebased on improved SMC.

The output of the SMC section is:

$$u = \frac{1}{b}(-ax - c - \varepsilon_1 \text{sgns} - \varepsilon_2 s) \quad (\varepsilon_1 > 0, \varepsilon_2 > 0) \tag{15}$$

According to the arrival conditions of the SMC, combining with formula (11):

$$s\dot{s} = -s[\varepsilon_2 s + \varepsilon_1 \text{sgn}(s)] = -\varepsilon_2 s^2 - \varepsilon_1 |s| \tag{16}$$

Because $\varepsilon_1 > 0, \varepsilon_2 > 0$, then $s\dot{s} < 0$, the Lyapunov function is:

$$V(x) = \frac{1}{2}s^2 \tag{17}$$

Combining formula (16) and formula (17), the expression is:

$$\dot{V}(x) = s\dot{s} = -\varepsilon_2 s^2 - \varepsilon_1 |s| < 0 \tag{18}$$

According to the above formula, $\dot{V}(x) < 0$ is established for any $\varepsilon_1 > 0, \varepsilon_2 > 0$, which can prove that the exponential SMC approach rate used in the set design torque link is gradually stable under the Lyapunov function.

In the design of the BLDCM DTC system, the set mode of the torque is usually obtained by the PI adjustment of the rotation speed error. This control mode is relatively simple, but the response speed is slow, and the robustness of the control system also needs to be improved. Synovial variable structure idea can effectively reduce the above defects, but also brings the problem of the system. In order to reduce the influence of vibration and improve the control accuracy, this design adopts integral sliding surface instead of the traditional linear sliding surface, which can optimize the continuity of the sliding mode variable structure and reduce the high frequency disturbance, thus reduce the sliding mode vibration, achieve smooth torque, and reduce the system steady-state error at the same time.

e is defined as the difference between the set speed ω^* and the actual speed ω. Take the state variable x_1 as the speed error value and the state variable x_2 as the corresponding integral:

$$\begin{cases} x_1 = \omega^* - \omega \\ x_2 = \int_0^t (\omega^* - \omega)dt = \int_0^t x_1 dt \end{cases} \tag{19}$$

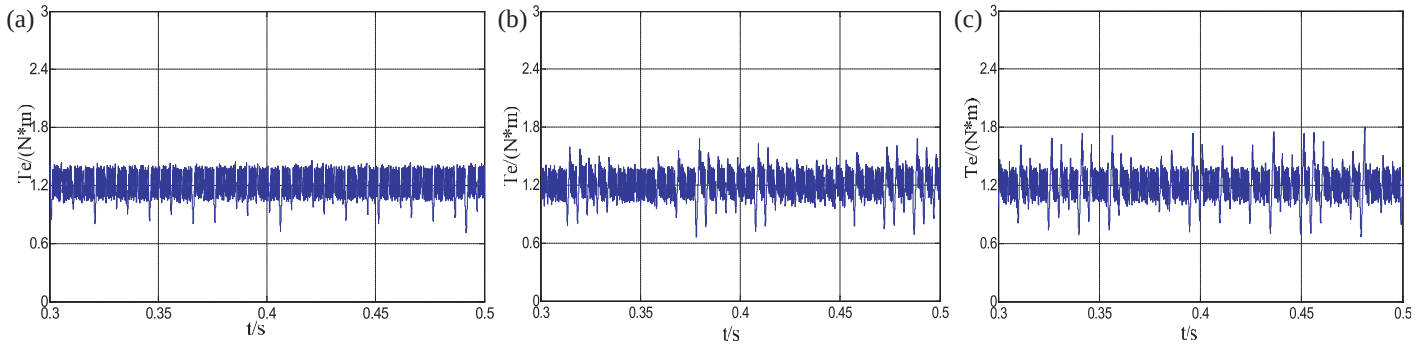

FIGURE 11. Torque waveform comparison at stable operation. (a) Based on the improved SMC torque waveform. (b) Based on the traditional SMC torque waveform. (c) Based on the PI torque waveform.

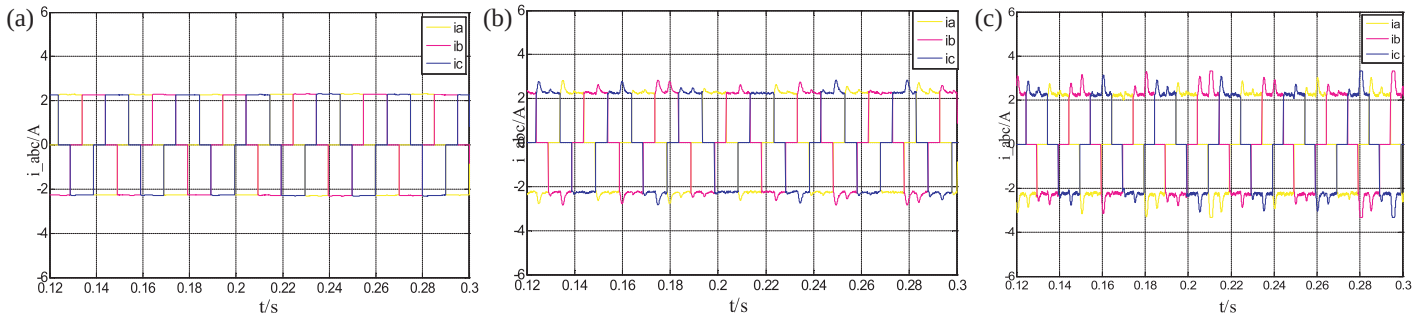

FIGURE 12. Reference current waveform comparison at stable operation. (a) Based on the improved SMC reference current. (b) Based on the traditional SMC reference current. (c) Based on the PI reference current.

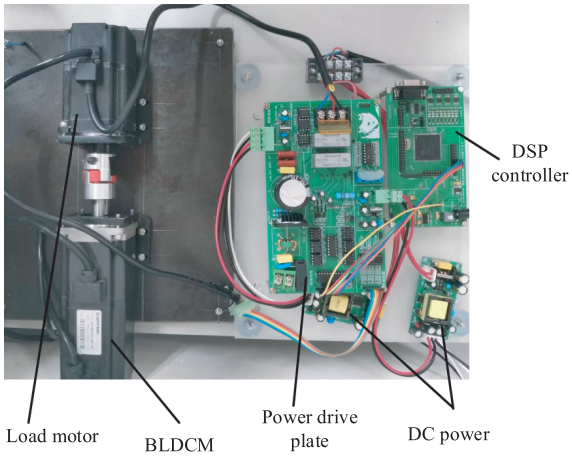

FIGURE 13. Experimental test bed.

Combining with formula (7), the derivative of the state variable x_1:

$$\begin{aligned}\dot{x}_1 &= \dot{\omega}^* - \dot{\omega} = \frac{B}{J}w - \frac{1}{J}Te + \frac{1}{J}TL \\ &= -\frac{B}{J}x_1 - \frac{1}{J}Te + \frac{1}{J}TL + \frac{B}{J}\omega^* \end{aligned} \tag{20}$$

where u is the sliding mode output torque T_e, and define $M = -\frac{B}{J}$, $N = -\frac{1}{J}$, $K = \frac{1}{J}TL + \frac{B}{J}\omega^*$; therefore, Equation (20) can be written as Equation (21). Combining with formula (19):

$$\begin{cases} \dot{x}_1 = Mx_1 + Nu + K \\ \dot{x}_2 = x_1 = \omega^* - \omega \end{cases} \tag{21}$$

The integral sliding mode surface is designed as:

$$s = x_1 + k\int_0^t x_1 dt = x_1 + kx_2 \tag{22}$$

In the above equation, the coefficient k is a normal number, and its size value determines the speed of the system approaching a stable state. The larger the k is, the faster the speed is, and the smaller the time is required to adjust the speed. However, excessive k value will lead to an integral saturation phenomenon, which will increase the time required for the system to finally stabilize.

Combining with formula (22):

$$\dot{s} = \dot{x}_1 + k\dot{x}_2 = \dot{x}_1 + kx_1 = Hx_1 + Nu + K \tag{23}$$

where $H = M + K$, make $s = \dot{s} = 0$, combining with formula (22):

$$x_1 = \omega^* - \omega = k_0 e^{-kt} \tag{24}$$

When the time tends to infinity, the state variable x_1 tends to 0, and the moving point slides towards the coordinate origin at the rate of e^{-kt}. Making $\dot{s} = 0$, the available equivalent control

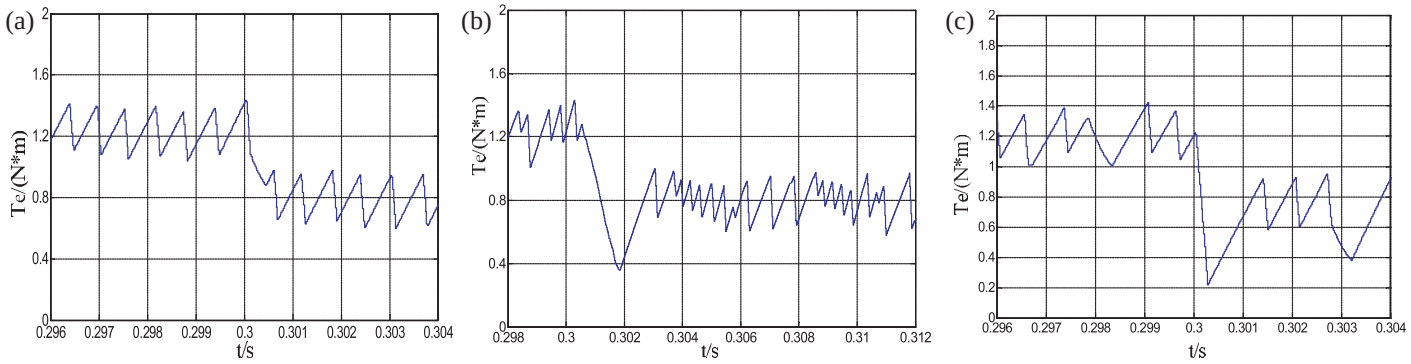

FIGURE 14. Torque response waveform in improved SMC control mode and PI control mode and traditional SMC control. (a) The torque mutation amplification waveform based on the improved SMC. (b) The torque mutation amplification waveform based on the PI control. (c) The torque mutation amplification waveform based on the traditional SMC control.

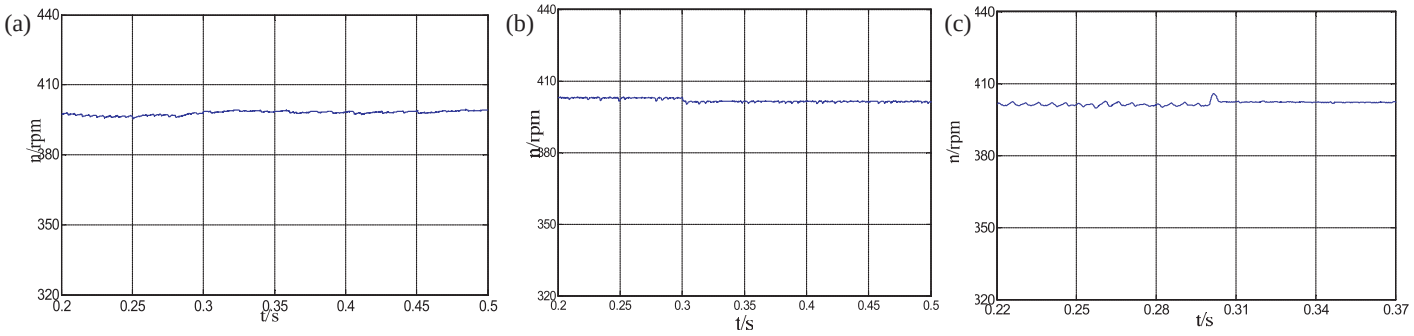

FIGURE 15. Speed response waveform in improved SMC control mode and the traditional SMC control. (a) the rotational speed response waveform of the improved SMC control mode. (b) the rotational speed response waveform of the traditional SMC control mode. (c) the rotational speed response waveform of the PI control.

rate is:

$$u_{eq} = -\frac{H}{N}x_1 - \frac{K}{N} \tag{25}$$

3. SIMULATION ANALYSIS

Based on the above analysis of the set sliding mode scheme of the torque, and the modeling analysis of the BLDCM DTC system in MATlAB/SIMULINK, the basic parameters of the BLDCM are shown in Table 1. Figure 1 shows the SIMULINK model of the DTC control system established by the BLDCM.

Figure 1 is the overall simulation model established for the BLDCM DTC system, which mainly includes the inverter module, BLDCM module, flux linkage calculation module, flux linkage set module, torque set module, and direct torque control module. In a BLDCM DTC system with the new flux linkage set mode, the improved sliding mode variable structure control is used to replace the traditional PI control and to realize the new torque set mode. The corresponding sliding mode control module is shown in Figure 2, in which the values of the parameters k, α, β, and δ of the sliding mode controller are 80, 0.35, 1, and 0.05, respectively.

Figures 3–9 are the simulation waveform diagrams of the BLDCM when the load torque is $1.2\,\mathrm{N}\cdot\mathrm{m}$ at a rated speed of 400 rpm, with a simulation time of 0.5 s and a step length of 0.01 ms. Under the integrated sliding mode control mode of the improved approach rate, the corresponding trajectories of the rotor flux linkage and integrated stator flux linkage vector are shown in Figures 3–7, respectively. Figure 5 shows the trajectory of the armature reaction flux linkage under a constant torque and during the torque mutation under the improved SMC control mode. Figure 6 shows the trajectory of the armature reaction flux linkage under a constant torque and during the torque mutation under the traditional SMC control mode. Figure 8 shows a three-phase waveform diagram of the current while in stable operation. Figures 9 and 10 show the corresponding rotational speed and torque response curves, respectively. Figure 11 shows the torque contrast curve under control in the three modes.

The magnetic vector trajectory shown in Figures 3–7 above verifies the effectiveness of the new flux linkage set method in the SMC-based control system. Since the set torque is based on the improved SMC, the maximum starting torque is $7\,\mathrm{N}\cdot\mathrm{m}$, so the actual value is large at the beginning. When the torque stabilizes to $1.2\,\mathrm{N}\cdot\mathrm{m}$, the flux linkage trajectory also converges to the stable zigzag trajectory, and the corresponding armature reaction flux linkage also converges to the closed hexagonal trajectory. By comparing Figures 5 and 6, it can be found that

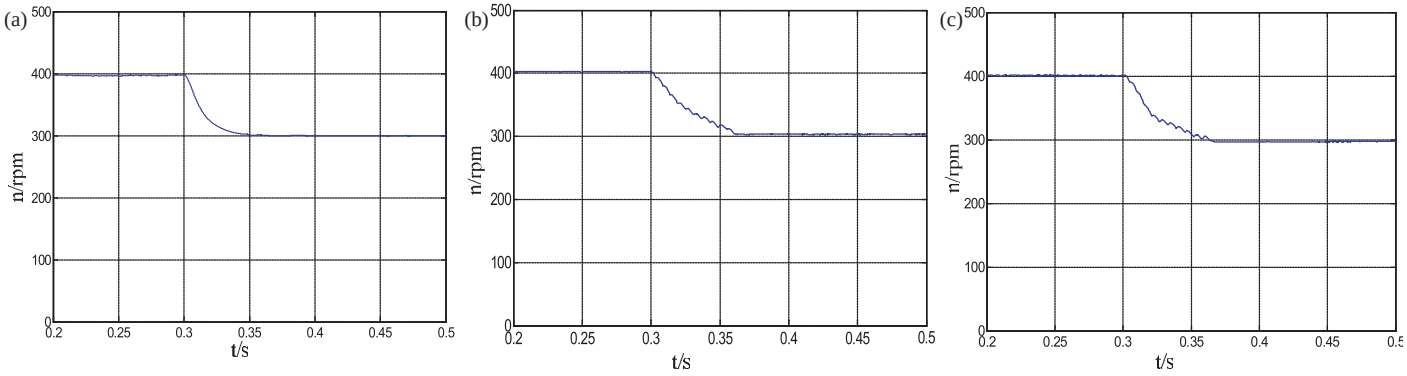

FIGURE 16. Speed response waveform when speed is abrupt. (a) The rotational speed response waveform based on the improved SMC. (b) The rotational speed response waveform based on the traditional SMC. (c) The rotational speed response waveform based on the PI.

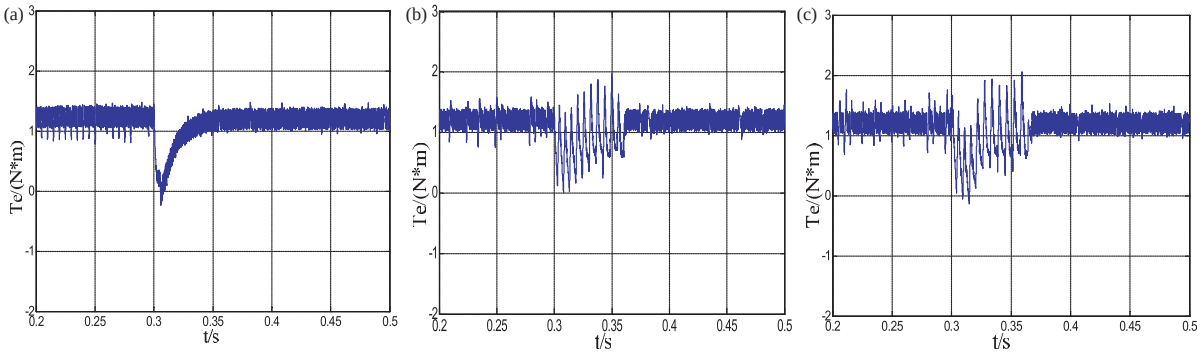

FIGURE 17. Torque response waveform when speed is abrupt. (a) The torque response waveform based on the improved SMC. (b) The torque response waveform based on the traditional SMC. (c) The torque response waveform based on the PI.

under the improved SMC control mode, the armature flux linkage trajectory distortion is greatly reduced at the six top angles of the hexagon, and the armature flux linkage distortion is the largest under the PI control mode. Therefore, it is shown that under the improved torque set mode, the torque pulsation is greatly reduced. The pulsation situation of the electromagnetic torque waveform in the three control modes shown in Figure 11 verifies the correctness of the actual torque pulsation inference mentioned above [10]. As can be seen from the smooth top of the reference current waveform in the three control modes shown in Figure 12, the set reference current rectangular wave is smoother under the set torque of the improved SMC. Combined with the ratio relationship with the set reference current, the set torque of the improved SMC is the most stable, and the set torque pulsation under the PI control is the largest. The three-phase current waveform compared with Figure 8 also shows that the current flat tip is smoother under the improved SMC control mode. From the speed torque response curve shown in Figures 9 and 10, compared with the PI control mode, the rotational speed response curve of the improved SMC control mode is smoother, and the response time is reduced to 0.08 s, showing a better static response performance.

4. EXPERIMENTAL RESULTS

As shown in Figure 13, the direct torque control system experiment platform of BLDCM with DSP controller as the core is built in this paper. The experimental platform is composed of BLDCM, DSP controller, power drive plate, DC power, load motor, etc. The PWM modulation mode is used during the experiment. The PWM modulation carrier frequency is 20 kHz, and the pulse period is set to 0.02 s. When the incoming magnetic current is 0.1 A, the set load torque is 1 N · m.

When the system runs to 0.3 s, the load torque decreases from 1.2 N · m to 0.8 N · m, and the corresponding electromagnetic torque and rotational speed waveform under the improved SMC control mode are shown in Figures 14 and 15, respectively. The system is able to respond quickly with a adjustment time of 0.0005 s and almost no change in speed. Combining with the traditional SMC control mode and the PI control mode shown in Figures 14 and 15, it can be seen that the improved SMC control mode responds more quickly and fluctuates less torque. Compared with the torque response waveform under the PI control mode, it can be seen that the improved SMC control mode system responds more quickly and smoothly.

When the system runs to 0.3 s, the set rotation speed is reduced from 400 rpm to 300 rpm, and the corresponding electromagnetic torque and rotational speed waveform comparison under the three control modes are shown in Figure 16 and Figure 17, respectively. It can be seen that the speed of the im-

TABLE 2. Comparison of dynamic and static response of different kinds of torque set.

The way of torque set	t_r (s)	t_s (s)	δ_1 (%)	t_T (ms)	Δn_1 (rpm)	t_n (s)
PI	0.112	0.112	0	1	1	0.077
The traditional SMC	0.112	0.112	0	1	0	0.060
The improved SMC	0.080	0.080	0	0.5	0	0.040

proved SMC control mode can land smoothly to 300 rpm in only 0.4 s, while the recovery time under the traditional SMC and PI control are 0.6 s and 0.77 s, respectively, and the torque jitter is large.

Based on the above analysis, in the BLDCM DTC control system under the set mode of the new flux linkage, the system not only has faster response speed, but also has stronger interference-resistance, and shows stronger dynamic and static performance. The dynamic and static response indicators under the control mode are summarized in Table 2, where t_r, t_s, and δ_1 respectively indicate the rise time, stability time, and overshoot when the motor is started under the same parameter setting conditions. When the load torque is reduced from $1.2\,\mathrm{N}\cdot\mathrm{m}$ to $0.8\,\mathrm{N}\cdot\mathrm{m}$, the system stability time and the maximum rotational speed increase are indicated by t_T and Δn_1, respectively. The stabilization time of the system when the rotational speed is mutated from 400 rpm to 300 rpm is indicated by t_n.

5. CONCLUSION

Aiming at the problem of slow response speed and poor anti-interference ability using the traditional PI control, this paper presents the brushless DC motor direct torque control based on sliding mode change structure. Using the integral sliding mode surface instead of the traditional linear sliding mode surface, the continuity of the sliding mode change structure is optimized, and the high frequency perturbation caused by the differential phase is reduced, thus reducing the sliding mode shaking while achieving the smooth torque, and the steady-state error of the system is reduced. The system is simulated by MATLAB/SIMULINK, and the set torque of the improved SMC is the most stable, while under the improved SMC control mode, the speed response curve is smoother, and the response time is reduced to 0.08 s, showing better static response performance. Through the construction of BLDCM test platform, the experimental results show that in the BLDCM DTC control system of the new flux linkage based on the improved SMC, the system not only has faster response speed, but also has stronger interference-resistance, and shows stronger dynamic and static performance.

REFERENCES

[1] Khazaee, A., H. A. Zarchi, G. A. Markadeh, and H. M. Hesar, "MTPA strategy for direct torque control of brushless DC motor drive," *IEEE Transactions on Industrial Electronics*, Vol. 68, No. 8, 6692–6700, Aug. 2021.

[2] De Castro, A. G., W. C. A. Pereira, T. E. P. de Almeida, et al., "Improved finite control-set model-based direct power control of BLDC motor with reduced torque ripple," *IEEE Transactions on Industry Applications*, Vol. 54, No. 5, 4476–4484, Sept. 2018.

[3] Zhou, Y., D. Zhang, X. Chen, and Q. Lin, "Sensorless direct torque control for saliency permanent magnet brushless DC motors," *IEEE Transactions on Energy Conversion*, Vol. 31, No. 2, 446–454, Jun. 2016.

[4] Maharajan, M. P. and S. A. E. Xavier, "Design of speed control and reduction of torque ripple factor in BLdc motor using spider based controller," *IEEE Transactions on Power Electronics*, Vol. 34, No. 8, 7826–7837, Aug. 2019.

[5] De Toledo, H. and J. L. Azcue, "Direct power control with space vector modulation applied for the brushless DC motor," *2019 IEEE 15th Brazilian Power Electronics Conference and 5th IEEE Southern Power Electronics Conference (COBEP/SPEC)*, 1–6, 2019.

[6] Akshay, R. S. R. and M. A. Chaudhari, "Direct torque control of PM BLDC motor using fuzzy controllers," *2017 International Conference on Innovations in Information, Embedded and Communication Systems (ICIIECS)*, 1–6, 2017.

[7] Narasimha Rao, C. N. and G. DurgaSukumar, "Analysis of torque ripple in vector control of BLDC motor using SVPWM technique," *2020 4th International Conference on Electronics, Communication and Aerospace Technology (ICECA)*, 519–523, 2020.

[8] Rajani, B., K. V. Rao, and R. Srinivas, "DC link voltage stabilization in renewable source connected DC micro grid using adaptive sliding mode controller," *2021 Emerging Trends in Industry 4.0 (ETI 4.0)*, 1–6, 2021.

[9] Hafez, A. T., A. A. Sarhan, and S. Givigi, "Brushless DC motor speed control based on advanced Sliding Mode Control (SMC) techniques," *2019 IEEE International Systems Conference (SysCon)*, 1–6, 2019.

[10] Putra, E. H., Z. Has, and M. Effendy, "Robust adaptive sliding mode control design with genetic algorithm for brushless DC motor," *2018 5th International Conference on Electrical Engineering, Computer Science and Informatics (EECSI)*, 2018.

[11] Ma, H., J. F. Yang, Y. P. Dou, et al., "A simple control method for direct torque control of BLDCM with low resolution hall sensors," *2018 21st International Conference on Electrical Machines and Systems (ICEMS)*, 493–496, 2018.

[12] Lee, K., F. Li, and W. Yao, "Comparative performance evaluation of hall effect sensorless control options in permanent magnet brushless DC motor drives," *2019 IEEE International Electric Machines & Drives Conference (IEMDC)*, 1110–1117, 2019.

[13] Aghili, F., "Ripple suppression of BLDC motors with finite driver/amplifer bandwidth at high velocity," *IEEE Transactions on Control Systems Technology*, Vol. 19, No. 2, 391–397, 2011.

[14] Fang, J., "Torque ripple reduction in BLDC torque motor with nonideal back EMF," *IEEE Transactions on Power Electronics*, Vol. 27, No. 11, 4630–4637, 2012.

[15] Guo, H., B. Zhou, G. Zuo, et al., "Adaptive sliding-mode observer for back electromotive force estimation of brushless DC motror," *Proceedings of the CSEE*, 2011.